

Kinetics of Radical Intermediate Formation and Deoxynucleotide Production in 3-Aminotyrosine-Substituted *Escherichia coli* Ribonucleotide Reductases

Ellen C. Minnihhan,[†] Mohammad R. Seyedsayamdost,^{†,‡} Ulla Uhlin,[§] and JoAnne Stubbe^{*,†,||}

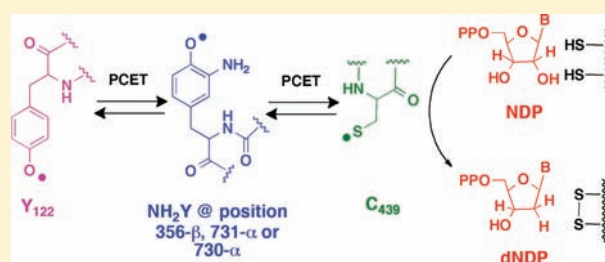
[†]Department of Chemistry and ^{||}Department of Biology, Massachusetts Institute of Technology, 77 Massachusetts Avenue, Cambridge, Massachusetts 02139, United States

[§]Department of Molecular Biology, Swedish University of Agricultural Science, Uppsala Biomedical Center, Box 590, SE-75124 Uppsala, Sweden

Supporting Information

ABSTRACT: *Escherichia coli* ribonucleotide reductase is an $\alpha\beta$ 2 complex and catalyzes the conversion of nucleoside 5'-diphosphates (NDPs) to 2'-deoxynucleotides (dNDPs). The reaction is initiated by the transient oxidation of an active-site cysteine (C₄₃₉) in α 2 by a stable diferric tyrosyl radical (Y₁₂₂•) cofactor in β 2. This oxidation occurs by a mechanism of long-range proton-coupled electron transfer (PCET) over 35 Å through a specific pathway of residues: Y₁₂₂• → W₄₈ → Y₃₅₆ in β 2 to Y₇₃₁ → Y₇₃₀ → C₄₃₉ in α 2. To study the details of this process, 3-aminotyrosine (NH₂Y) has been site-specifically incorporated in place of Y₃₅₆ of β .

The resulting protein, Y₃₅₆NH₂Y- β 2, and the previously generated proteins Y₇₃₁NH₂Y- α 2 and Y₇₃₀NH₂Y- α 2 (NH₂Y-RNRs) are shown to catalyze dNDP production in the presence of the second subunit, substrate (S), and allosteric effector (E) with turnover numbers of 0.2–0.7 s⁻¹. Evidence acquired by three different methods indicates that the catalytic activity is inherent to NH₂Y-RNRs and not the result of copurifying wt enzyme. The kinetics of formation of 3-aminotyrosyl radical (NH₂Y•) at position 356, 731, and 730 have been measured with all S/E pairs. In all cases, NH₂Y• formation is biphasic (k_{fast} of 9–46 s⁻¹ and k_{slow} of 1.5–5.0 s⁻¹) and kinetically competent to be an intermediate in nucleotide reduction. The slow phase is proposed to report on the conformational gating of NH₂Y• formation, while the k_{cat} of ~0.5 s⁻¹ is proposed to be associated with rate-limiting oxidation by NH₂Y• of the subsequent amino acid on the pathway during forward PCET. The X-ray crystal structures of Y₇₃₀NH₂Y- α 2 and Y₇₃₁NH₂Y- α 2 have been solved and indicate minimal structural changes relative to wt- α 2. From the data, a kinetic model for PCET along the radical propagation pathway is proposed.



INTRODUCTION

The class Ia ribonucleotide reductase (RNR) from *Escherichia coli* catalyzes the reduction of four nucleoside 5'-diphosphate substrates (S, where S is UDP, CDP, ADP and GDP) to 2'-deoxynucleoside 5'-diphosphates (dNDPs) in a highly orchestrated fashion.^{1–3} Allosteric effectors (E, where E is ATP, dGTP, TTP, and dATP) bind to the specificity site (S-site) and ATP/dATP bind to the activity site (A-site), dictating the substrate reduced and the overall enzyme activity, respectively. The active site and both allosteric sites are located in α 2, whereas the essential diferric tyrosyl radical (Y₁₂₂• in *E. coli*) cofactor resides in β 2. This stable Y• serves as the radical initiator for the transient oxidation of the active-site cysteine (C₄₃₉) in α 2 which initiates nucleotide reduction.

The active form of the *E. coli* RNR is proposed to be an $\alpha\beta$ 2 complex.⁴ While the individual structures of α 2 and β 2 have been solved, no structure of the $\alpha\beta$ 2 complex has been determined to date. Thus, a docking model of the two subunits has been generated based on shape complementarity of the individual

subunits, the superposition of their 2-fold symmetry axes, and the relative locations of strictly conserved residues.⁵ The most provocative feature of the docking model is the 35 Å distance it places between the redox-coupled residues C₄₃₉ in α 2 and Y₁₂₂• in β 2.⁵ Uhlin and Eklund proposed a mechanism to rationalize this long-range oxidation in which conserved, redox-active aromatic amino acids constitute a specific pathway for radical propagation: Y₁₂₂• → W₄₈ → Y₃₅₆ in β 2 to Y₇₃₁ → Y₇₃₀ → C₄₃₉ in α 2. Our hypothesis for radical propagation (Figure 1) has developed from this original model, and invokes orthogonal proton-coupled electron transfer (PCET) within β 2 and co-linear PCET within α 2.⁶ In the advent of emerging technology for the site-specific incorporation of unnatural amino acids into proteins, we have begun to provide convincing evidence in support of this hypothesis.

Studies from our laboratory have established that the rate-limiting step in NDP reduction in wt *E. coli* RNR is associated

Received: February 21, 2011

Published: May 25, 2011

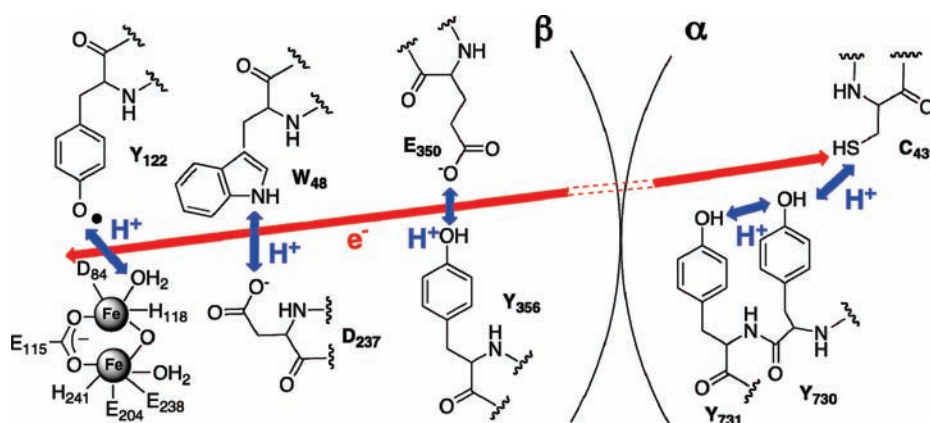


Figure 1. Stubbe/Nocera model for long-range (~ 35 Å), reversible PCET by a radical hopping mechanism in *E. coli* class Ia RNR. Evidence suggests orthogonal PCET is operative in the β subunit, and co-linear PCET is operative in the α subunit. Residue Y_{356} has not been observed in any crystal structure of $\beta 2$, and thus its location relative to the other residues is unknown.

with conformational changes triggered by binding of S and E to $\alpha 2$.⁷ These changes occur prior to radical propagation, are intricately linked to its initiation, and mask observation of any radical intermediates generated during long-range propagation.⁷ To study the details of this process and to characterize radical intermediates, our laboratory has focused on subtly perturbing the wt enzyme through the site-specific incorporation of tyrosine analogs with different reduction potentials and/or phenolic pK_a s in place of the Ys on the pathway. Studies conducted on these mutants have provided evidence for our working model shown in Figure 1.

The role of Y_{356} in $\beta 2$ has been studied most extensively, with more than a half dozen tyrosine analogs substituted at this position using expressed protein ligation (EPL). These include the thermodynamic radical trap 2,3-dihydroxyphenylalanine (DOPA),^{8,9} the radical block and pK_a probe 3-nitrotyrosine (NO_2Y),^{10,11} and the dual pK_a /reduction potential reporter fluorotyrosines (F_nYs , $n = 1-4$).^{12,13} The data from these studies have provided convincing evidence that Y_{356} is a redox-active participant on the pathway. This result is particularly important as the C-terminal 35 amino acids of β , including Y_{356} , constitute a thermally disordered tail that provides key recognition features for the $\alpha 2/\beta 2$ interaction.¹⁴ The docking model predicts a distance of >25 Å between W_{48} in $\beta 2$ and Y_{731} in $\alpha 2$ (Figure 1), and our collective results support the participation of Y_{356} as a relay between these two residues across the subunit interface.

More recently, Y_{730} and Y_{731} of $\alpha 2$ have been targeted for site-specific replacement using the *in vivo* nonsense codon suppression technology.¹⁵ Employing a specific, orthogonal tRNA/tRNA-synthetase (RS) pair, the radical trap 3-aminotyrosine (NH_2Y , $E^{o'} \approx 0.64$ V, pH 7)¹⁶ was incorporated into each position.^{17,18} When combined with $\beta 2$, CDP, and ATP, $Y_{730}NH_2Y-\alpha 2$ (or $Y_{731}NH_2Y-\alpha 2$) generated an aminotyrosyl radical ($NH_2Y\bullet$) in a kinetically competent fashion. These studies, in conjunction with complementary studies of the “off-pathway” mutant $Y_{413}NH_2Y-\alpha 2$, provided evidence for a specific radical propagation pathway in α , involving Y_{730} and Y_{731} .^{17,19} Our initial results also reported that both $Y_{730}NH_2Y-\alpha 2$ and $Y_{731}NH_2Y-\alpha 2$ were active in dNDP formation and thus indicated that the decrease in reduction potential of NH_2Y relative to Y is insufficient to shut down radical propagation. Using an E_p for Y of ~ 0.83 V (pH 7),²⁰ the difference

between Y and NH_2Y is estimated to be ~ 190 mV; however, potentials up to 0.93 V have been reported for Y,¹⁶ suggesting the difference may be greater. The activities of $NH_2Y-\alpha 2$ s were surprising, as this observation contrasts with previous studies on $Y_{356}DOPA-\beta 2$ ($E^{o'} \approx 0.57$ V, pH 7),²¹ for which no catalytic activity was detectable ($<1/10^4$ wt).⁸ Additionally, our previous studies on $Y_{356}NO_2Y-\beta 2$ and $Y_{356}F_nY-\beta 2$ s indicated that a 200 mV increase in potential relative to Y is sufficient to shut down nucleotide reduction.^{10,13}

In this work, we report the expression, isolation, and characterization of $Y_{356}NH_2Y-\beta 2$. This is the first mutant at position 356 of $\beta 2$ generated by the *in vivo* nonsense suppression method. The data obtained with this mutant is free of many of the complexities described previously for the EPL-generated mutant $\beta 2$ s, in which two additional mutations were required to make sufficient protein for biophysical studies.¹⁰ As was previously observed with $NH_2Y-\alpha 2$ s, $Y_{356}NH_2Y-\beta 2$ catalyzes dNDP production. Steady-state assays of NH_2Y -RNRs demonstrate they possess 3–12% the activity of the respective wt subunit ($k_{obs} \approx 0.2-0.7$ s⁻¹). Three types of experiments were conducted to establish that the catalytic activity measured is associated with the NH_2Y -RNRs and not with contaminating wt enzyme that copurifies with each mutant. The X-ray crystal structures of $Y_{730}NH_2Y-\alpha 2$ and $Y_{731}NH_2Y-\alpha 2$ have been solved and demonstrate that NH_2Y introduces minimal perturbation to the structural integrity of $\alpha 2$ and the conformation of residues involved in radical propagation.

The kinetics of $NH_2Y\bullet$ formation have been examined with each of the three NH_2Y -RNRs in the presence of the physiologically relevant S/E pairs and are all biphasic. The slower phase is invariant with position of NH_2Y in the pathway and with the S/E pair studied, and is proposed to report on the rate-limiting conformational change in the wt enzyme. A comparison of the rate constants for $NH_2Y\bullet$ formation with S or E alone indicates that S is responsible for triggering radical propagation. From these studies, a general model is proposed for long distance radical propagation that may be used to understand mechanistic details of this process relevant to the wt enzyme.

■ MATERIALS AND METHODS

Materials. Wt- $\alpha 2$ (2500 nmol/min/mg) and wt- $\beta 2$ (1.2 $Y_{122}\bullet/\beta 2$, 7600 nmol/min/mg) were expressed from pMJ1-*nrda*

and pTB2-*nrdB*, respectively, and purified as previously described.^{22,23} $Y_{731}NH_2Y-\alpha_2$ and $Y_{730}NH_2Y-\alpha_2$ were coexpressed from pTrc-*nrdA*-TAG₇₃₁ or pTrc-*nrdA*-TAG₇₃₀ and pAC-NH₂Y, and purified as described.¹⁷ All α_2 proteins were prereduced prior to use.¹⁷ *E. coli* thioredoxin (TR, 40 U/mg) and thioredoxin reductase (TRR, 1400 U/mg) were isolated as described.^{24,25} 2'-Azido-2'-deoxycytidine 5'-diphosphate (N₃CDP) was synthesized from uridine by known procedures.^{26,27} [^{5-³H}]-CDP was purchased from ViTrax (Placentia, CA). Nucleotide primers were purchased from Invitrogen, *Pfu* Ultra II polymerase from Stratagene, and restriction enzymes from New England Biolabs. Assay buffer consists of 50 mM Hepes, 1 mM EDTA, and 15 mM MgSO₄, pH 7.6. Generation of pTrc-*nrdB*, pTrc-*nrdB*(TAG₃₅₆), pET-*nrdA*(wt), pET-*nrdA*(TAG₇₃₀), and pEVOL-NH₂Y, and expression and purification of N-Strep- $Y_{730}NH_2Y-\alpha_2$, N-Strep- $Y_{356}NH_2Y-\beta_2$, and (His)₆- $Y_{356}NH_2Y-\beta_2$ are described in detail in the Supporting Information (SI).

Expression and Purification of $Y_{356}NH_2Y-\beta_2$. $Y_{356}NH_2Y-\beta_2$ was expressed in *E. coli* DH10B cells (Invitrogen) from pTrc-*nrdB*(TAG₃₅₆) and pAC-NH₂Y in a fashion identical to that of NH₂Y-substituted α_2 s¹⁷ and gave ~1.5 g wet cell paste per L of culture. Purification by the previously reported protocol^{11,22} using two anion exchange chromatography steps gave a mixture of three species: β'_2 (where β' is β truncated after residue 355), $Y_{356}NH_2Y-\beta\beta'$, and $Y_{356}NH_2Y-\beta_2$.

Fractions containing primarily full-length $Y_{356}NH_2Y-\beta_2$ were pooled, concentrated using a YM-30 membrane (Amicon), and subjected to FPLC on a Poros HQ/20 column (Applied Biosystems, 1.6 × 10 cm, 20 mL). The column was equilibrated in buffer B (50 mM Tris, 5% glycerol, pH 7.6) and was loaded with $Y_{356}NH_2Y-\beta_2$ (~20 mg). The column was washed with one column volume (CV) of 150 mM NaCl in buffer B at 1.5 mL/min, then eluted with a gradient of 150 mM to 450 mM NaCl (60 mL × 60 mL) at the same flow rate. This protocol gave $Y_{356}NH_2Y-\beta_2$ of >95% purity, as judged by SDS-PAGE. Protein contained ~0.3 $Y_{122}\bullet/\beta_2$ as isolated.

ESI-MS Characterization of $Y_{356}NH_2Y-\beta_2$. ESI-MS analysis was conducted at the Proteomics Core Facility in the Koch Center for Integrative Cancer Research (MIT). The protein was absorbed on a protein microtrap (Michrom BioResources) and desalted by HPLC (50% water/50% acetonitrile/0.1% formic acid) immediately prior to MS analysis. Molecular weight measurements were made by LC-MS on a QSTAR Elite quadrupole-TOF mass spectrometer, which had been externally calibrated to a resolution of ~50 ppm.

Iron Chelation and Reconstitution of Diferric $Y\bullet$ Cofactor in $Y_{356}NH_2Y-\beta_2$. FPLC-purified $Y_{356}NH_2Y-\beta_2$ (225 μ M, 1.0 mL, 0.3 $Y\bullet/\beta_2$) was placed in a pear-shaped flask fitted with a vacuum adaptor, degassed on a Schlenk line, and brought into an anaerobic chamber at 4 °C. Sodium dithionite and methyl viologen were added to the stirring protein solution to final concentrations of 8 mM and 20 μ M, respectively. The resulting pale blue solution was stirred for 1 h at 4 °C. A 50-fold molar excess of ferrozine was added, and the solution was stirred for an additional 15 min. The protein solution was removed from the anaerobic chamber, applied to a G-25 Sephadex column (45 mL), and eluted with reconstitution buffer (50 mM Hepes, 5% glycerol, pH 7.6). The protein-containing fractions were concentrated to give apo- $Y_{356}NH_2Y-\beta_2$ in >90% yield. The diferric $Y\bullet$ cofactor was then reconstituted as described.²⁸ Radical quantitation by UV-vis absorption and EPR spectroscopies indicated 0.5 $Y_{122}\bullet/\beta_2$.²⁸

Determining the Specific Activity of $Y_{356}NH_2Y-\beta_2$. The activity of $Y_{356}NH_2Y-\beta_2$ was determined using the spectrophotometric⁷ and radioactive assays.¹³ $Y_{356}NH_2Y-\beta_2$ (0.1 or 0.5 μ M) was assayed in the presence of a 5-fold excess of wt- α_2 (0.5 μ M or 2.5 μ M) in assay buffer at 25 °C with [^{5-³H}]-CDP (5500 cpm/nmol).

Expression, Purification, and Activity Assays of (His)₆- $Y_{730}NH_2Y-\alpha_2$. *E. coli* BL21(Star)-DE3 cells (Invitrogen) were cotransformed with pET-*nrdA*(TAG₇₃₀) and pEVOL-NH₂Y and plated on LB-agar plates with 50 μ g/mL kanamycin (Km) and 50 μ g/mL chloramphenicol (Cm) at 37 °C. Starter (5 mL) and intermediate (100 mL) cultures were grown in 2XYT at 37 °C with Km and Cm. Enriched GMMML¹⁷ (500 mL) with the appropriate antibiotics was inoculated with the saturated intermediate culture (1:50 dilution) and grown at 37 °C, 225 rpm until reaching an OD₆₀₀ ~0.75, at which point NH₂Y and DTT were added to the culture to concentrations of 1 mM and 0.1 mM, respectively. After 15 min, the NH₂Y-RS was induced with L-arabinose to a final concentration of 3.3 mM. After an additional 20 min, *nrdA* expression was induced with 1 mM IPTG. Cells were harvested by centrifugation 3.5 h after induction to give 2 g cell paste/L culture.

The cell pellet was resuspended in buffer H (50 mM sodium phosphate, 5% glycerol, pH 7.2) with 0.5 mM PMSF and 10 mM β -mercaptoethanol (β -ME) in 5 mL buffer/g cell paste, homogenized, and lysed via two passes through a French pressure cell at 14 000 psi. Cell debris was cleared by centrifugation (40 000 × *g*, 25 min, 4 °C), and DNase (NEB) was added to the supernatant at 10 U/mL. The resulting solution was incubated with rocking for 30 min at 4 °C. The supernatant was added to Ni-NTA agarose (Qiagen, 1 mL/g) and buffer H was adjusted to contain 300 mM NaCl. The resulting slurry was incubated with rocking for 1 h at 4 °C, then loaded into a column, which was washed with 15 CVs of wash buffer (buffer H with 300 mM NaCl and 10 mM imidazole, pH 7.2) with 0.5 mM PMSF and 10 mM β -ME. The protein was eluted with a linear gradient of 10 to 250 mM imidazole in wash buffer. Fractions were pooled, diluted with buffer H, and concentrated using an Amicon YM 30 membrane to give ≥ 5 mg/g cell paste.

The protein was subjected to anion-exchange FPLC to remove a small amount of copurifying 729-truncated α . A Poros HQ/20 column was equilibrated in assay buffer and was loaded with 10–20 mg of protein. The column was washed with one CV of assay buffer at a flow rate of 4 mL/min, then eluted with a linear gradient of 50 to 450 mM NaCl (60 mL × 60 mL) in the same buffer at the same flow rate. Fractions containing the desired protein, determined by SDS-PAGE, were pooled and concentrated with an Amicon YM-30 membrane. The activity of (His)₆- $Y_{730}NH_2Y-\alpha_2$ was determined using the radioactive assay.¹³

Characterization of NH₂Y \bullet Formation in (His)₆- $Y_{730}NH_2Y-\alpha_2$. The formation of NH₂Y \bullet in the reaction of (His)₆- $Y_{730}NH_2Y-\alpha_2$ with wt- β_2 , CDP, and ATP was studied by SF UV-vis absorption and EPR spectroscopy as described previously, as was the reaction between (His)₆- $Y_{730}NH_2Y-\alpha_2$, wt- β_2 , N₃CDP, and ATP.¹⁷

Crystal Structure Determination of $Y_{730}NH_2Y-\alpha_2$ and $Y_{731}NH_2Y-\alpha_2$. Proteins were crystallized at 4 °C using the hanging drop vapor diffusion method in EasyXtal Tool plates (Qiagen) in the presence of a 20-amino acid peptide corresponding to the C-terminus of the *E. coli* β .⁵ Hanging drops consisted of 2 μ L of a 1:1 mixture of protein (8–9 mg/mL, final concentration) and peptide (30 mg/mL) solutions in assay buffer

and 2 μL of a solution of 25 mM sodium citrate, 1.5 M LiSO_4 , 2 mM DTT, pH 6 to a final mixture pH of 6.0–6.5. Crystals were grown for one week in a cold room, washed with 1.5 M LiSO_4 in 20% ethylene glycol, mounted in fiber loops, and flash-frozen in liquid N_2 .

Data sets were collected at 100 K at the European Synchrotron Radiation Facility. A 2.3 Å structure of the *E. coli* wt $\alpha 2$ (PDB-ID 2x0x)¹¹ was used as the initial model for the refinement of data for the mutant proteins. Processing and scaling were done with the program MOSFLM/SCALA,²⁹ refinement with the program Refmac,³⁰ and model building with the program O.³¹ Additional details on data collection and refinement are given in Table S3 (SI). Structures have been deposited to the PDB with ID codes 2x04 ($\text{Y}_{730}\text{NH}_2\text{Y}-\alpha 2$) and 2x05 ($\text{Y}_{731}\text{NH}_2\text{Y}-\alpha 2$).

Reaction of $\text{Y}_{730}\text{NH}_2\text{Y}-\alpha 2$ (or $\text{Y}_{731}\text{NH}_2\text{Y}-\alpha 2$) and wt- $\beta 2$ with Various S/E Pairs Monitored by EPR Spectroscopy. Prerduced $\text{Y}_{730}\text{NH}_2\text{Y}-\alpha 2$ (or $\text{Y}_{731}\text{NH}_2\text{Y}-\alpha 2$) and E were mixed rapidly with $\beta 2$ and S in assay buffer at 25 °C. The reaction was hand-quenched at 20 s in liquid N_2 and its EPR spectrum recorded (see below). Reactions were carried out with 15 μM of each subunit and the following S/E pairs: CDP/ATP (1 mM, 3 mM), GDP/TTP (1 mM, 0.2 mM), UDP/ATP (1 mM, 3 mM), and ADP/dGTP/ATP (1 mM, 0.2 mM, 3 mM). The reaction between (His)₆- $\text{Y}_{730}\text{NH}_2\text{Y}-\alpha 2$ and wt- $\beta 2$ with CDP/ATP was studied in an identical fashion.

EPR spectra were recorded at 77 K on a Bruker EMX X-band spectrometer equipped with a quartz finger dewar containing liquid N_2 in the Department of Chemistry Instrumentation Facility. EPR parameters were as follows: microwave frequency = 9.34 GHz, power = 30 μW , modulation amplitude = 1.5 G, modulation frequency = 100 kHz, time constant = 5.12 ms, scan time = 41.9 s. Spin quantitation and analysis of composite reaction spectra were carried out as described previously.¹⁷

Reaction of $\text{Y}_{730}\text{NH}_2\text{Y}-\alpha 2$ (or $\text{Y}_{731}\text{NH}_2\text{Y}-\alpha 2$) and wt- $\beta 2$ with S, E, or S/E Pairs Monitored by Stopped-Flow (SF) UV-Vis spectroscopy. SF kinetics were performed on an Applied Photophysics DX 17MV instrument equipped with the Pro-Data upgrade. All reactions were carried out in assay buffer at 25 °C. In all cases, prerduced $\text{Y}_{730}\text{NH}_2\text{Y}-\alpha 2$ (or $\text{Y}_{731}\text{NH}_2\text{Y}-\alpha 2$) and E (if present) in one syringe were mixed rapidly with $\beta 2$ and S (if present) in a second syringe to yield a final concentration of 5 μM $\text{NH}_2\text{Y}-\alpha 2/\beta 2$. The following S and/or E combinations (final concentrations) were studied: CDP/ATP (1 mM, 3 mM), GDP/TTP (1 mM, 0.2 mM), UDP/ATP (1 or 2 mM, 3 mM), ADP/dGTP (1 mM, 0.2 mM), ADP/dGTP/ATP (1 mM, 0.2 mM, 3 mM), CDP (1 mM), GDP (1 mM), UDP (1 mM), ADP (1 mM), ATP (3 mM), TTP (0.2 mM), and dGTP (0.2 mM). The reactions were monitored at 325 nm for $\text{NH}_2\text{Y}_{730}\bullet$ ($\epsilon \approx 10\,500\text{ M}^{-1}\text{ cm}^{-1}$) and 320 nm for $\text{NH}_2\text{Y}_{731}\bullet$ ($\epsilon \approx 11\,000\text{ M}^{-1}\text{ cm}^{-1}$) using PMT detection. Averaged kinetic traces generated from >5 individual traces were fit iteratively using OriginPro or KaleidaGraph software until residuals were minimized. The reaction between (His)₆- $\text{Y}_{730}\text{NH}_2\text{Y}-\alpha 2$ and wt- $\beta 2$ with CDP/ATP was examined in an analogous fashion.

Reaction of $\text{Y}_{356}\text{NH}_2\text{Y}-\beta 2$ and wt- $\alpha 2$ with Various S/E Pairs Monitored by SF UV-Vis and EPR Spectroscopy. SF UV-vis experiments were conducted by mixing $\text{Y}_{356}\text{NH}_2\text{Y}-\beta 2$ and prerduced wt- $\alpha 2$ in a 1:1 ratio (final concentration of 7.5–10 μM per subunit, 3.75–5 μM total $\text{Y}_{122}\bullet$) in the presence of one of the four S/E pairs or CDP alone, as described above. Reactions were monitored at 324 nm for $\text{NH}_2\text{Y}_{356}\bullet$ and 410 nm

for $\text{Y}_{122}\bullet$. Data analysis was conducted as described above. The reaction of $\text{Y}_{356}\text{NH}_2\text{Y}-\beta 2$ (25 μM) with wt- $\alpha 2$ (25 μM), CDP (1 mM) and ATP (3 mM) at 25 °C was hand-quenched at 20 s and analyzed by EPR spectroscopy as described above.

Reaction of $\text{Y}_{356}\text{NH}_2\text{Y}-\beta 2$, wt- $\alpha 2$, N_3CDP , and ATP Monitored by EPR Spectroscopy. Wt- $\alpha 2$ and ATP were mixed with $\text{Y}_{356}\text{NH}_2\text{Y}-\beta 2$ and N_3CDP in assay buffer to give final concentrations of 30 μM , 3 mM, 30 μM (15 μM $\text{Y}\bullet$), and 250 μM , respectively, in a reaction volume of 240 μL . The reaction mixture was incubated at 25 °C for 1 min, then hand-quenched in liquid N_2 . Acquisition of EPR spectra and spin quantitation were conducted as described above, and deconvolution of the three radical species was performed as described previously.¹⁷

Single-Turnover Reaction of $\text{NH}_2\text{Y}-\alpha 2$ s with wt- $\beta 2$, CDP, and ATP. In a total volume of 500 μL was combined wt- $\beta 2$ (10 μM), [³H]-CDP (0.3–0.5 mM, specific activity of 6700 or 21 300 cpm/nmol), and ATP (3 mM) in assay buffer at 25 °C. The assay was initiated by addition of prerduced $\alpha 2$ (wt, $\text{Y}_{730}\text{NH}_2\text{Y}-\alpha 2$, (His)₆- $\text{Y}_{730}\text{NH}_2\text{Y}-\alpha 2$, or $\text{Y}_{731}\text{NH}_2\text{Y}-\alpha 2$, 2.0 μM). The reaction was quenched in a boiling water bath after the time required to consume all the substrate under steady-state conditions. Sample workup and scintillation counting was conducted as described previously.¹³

RESULTS

Expression, Purification, and Characterization of $\text{Y}_{356}\text{NH}_2\text{Y}-\beta 2$. A number of expression systems, growth conditions, and purification techniques were investigated to maximize the production and isolation of full-length $\text{Y}_{356}\text{NH}_2\text{Y}-\beta 2$, generated by the *in vivo* nonsense codon suppression method. This method results in the expression of a mixture of full-length β (residues 1–375) and truncated β (1–355, designated β') and, since β is an obligate dimer, a statistical distribution of $\beta 2$, $\beta\beta'$, and $\beta'2$ is generated. Ultimately, the pTrc-*nrdB*(TAG₃₅₆) and pAC-NH₂Y¹⁷ expression system was chosen, as it resulted in the highest yield of purified $\text{Y}_{356}\text{NH}_2\text{Y}-\beta 2$. A purification protocol employing three anion-exchange chromatography steps was required to separate $\text{Y}_{356}\text{NH}_2\text{Y}-\beta 2$ from $\beta\beta'$ and $\beta'2$ and to isolate the desired species in >95% purity (Figure S1 of SI). ESI-MS analysis of the protein indicated a single major species of 43 402 Da (predicted 43 401 Da, Figure S2 of SI). Addition of variable amounts of wt- $\beta 2$ (predicted 43 386 Da) to $\text{Y}_{356}\text{NH}_2\text{Y}-\beta 2$ and analysis by ESI-MS allowed the lower limit of detection of contamination by wt- $\beta 2$ to be set to <5% the total $\text{Y}_{356}\text{NH}_2\text{Y}-\beta 2$.

The radical content of $\text{Y}_{356}\text{NH}_2\text{Y}-\beta 2$ as isolated was 0.3 $\text{Y}\bullet/\beta 2$. Efforts to increase the amount to levels observed in the wt enzyme (1.2 $\text{Y}\bullet/\beta 2$) via standard reconstitution methods resulted in a maximum of 0.5 $\text{Y}\bullet/\beta 2$. The reduced level of radical is likely associated with perturbation of the cofactor assembly pathway by the introduction of an easily oxidized Y analog at position 356. Similar results were observed in previous attempts to increase radical content in $\text{Y}_{356}\text{DOPA}-\beta 2$.^{8,32}

Characterization of $\text{NH}_2\text{Y}\bullet$ at Position 356. $\text{Y}_{356}\text{NH}_2\text{Y}-\beta 2$ was reacted with wt- $\alpha 2$, CDP, and ATP and the reaction quenched at 20 s and examined by EPR spectroscopy (Figure 2A). The reaction spectrum (black) is a composite of two radical species. Subtraction the $\text{Y}_{122}\bullet$ spectrum (red) yields a spectrum suggestive of an $\text{NH}_2\text{Y}\bullet$ (blue),³³ with more pronounced hyperfine features than observed for the $\text{NH}_2\text{Y}\bullet$ s at positions 730 and 731. Spin quantitation indicates 20% of the

total spin is lost during the reaction time with the remaining spin distributed between $\text{NH}_2\text{Y}\bullet$ (41%) and $\text{Y}\bullet$ (59%). Thus, 33% of the total spin at $t = 0$ was trapped as $\text{NH}_2\text{Y}\bullet$ at $t = 20$ s. For comparison, the reaction with $\text{Y}_{731}\text{NH}_2\text{Y}-\alpha 2$ gave 30% spin loss over 20 s, with the remaining radical distributed between $\text{NH}_2\text{Y}\bullet$ (45%) and $\text{Y}\bullet$ (55%).

The kinetics of $\text{NH}_2\text{Y}_{356}\bullet$ formation and $\text{Y}_{122}\bullet$ loss were examined under similar conditions by SF UV-vis spectroscopy (Figure 2B). The data were best fit to two exponentials, giving k_{fast} of 36 s^{-1} and k_{slow} of 2.1 s^{-1} . Twenty-five percent of the starting $\text{Y}\bullet$ was converted to $\text{NH}_2\text{Y}\bullet$ in the fast phase, and an additional 5% in the slow phase. A complete kinetic comparison

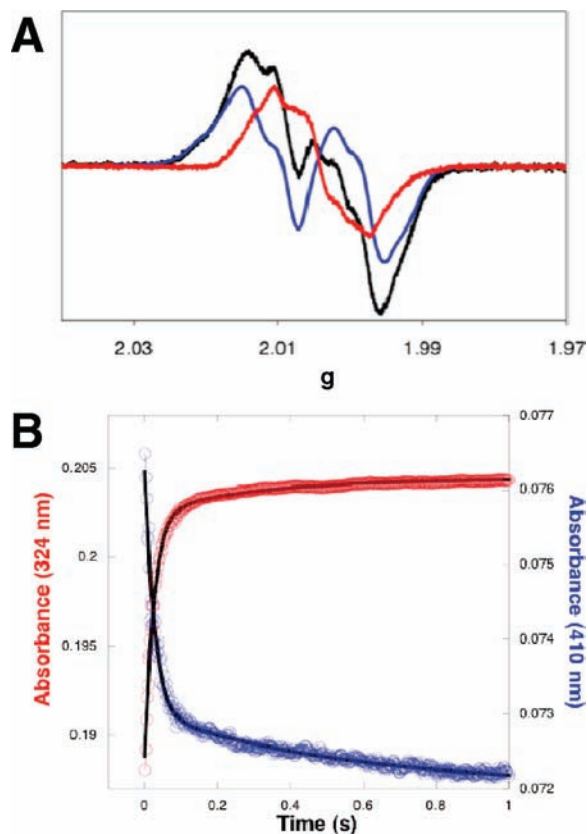


Figure 2. Reaction of $\text{Y}_{356}\text{NH}_2\text{Y}-\beta 2$ with wt- $\alpha 2$, CDP, and ATP. (A) EPR spectrum of the reaction mixture hand-quenched after incubation for 20 s at 25 °C. The reaction spectrum (black) is a composite of two species. Subtraction of a spectrum of the $\text{Y}_{122}\bullet$ (blue) gives the spectrum of the $\text{NH}_2\text{Y}_{356}\bullet$ (red). (B) SF UV-vis spectroscopy was used to determine the kinetics of $\text{NH}_2\text{Y}_{356}\bullet$ formation (324 nm, red) and $\text{Y}_{122}\bullet$ loss (410 nm, blue) under single-turnover conditions at 25 °C. Biexponential fits to the data are indicated by black lines.

Table 1. Nucleotide Reductase Activities of NH_2Y -RNRs

mutant	$\text{Y}\bullet/\beta 2$	spec act (nmol/min/mg) ^a	turnover (s ⁻¹)	activity (% wt) ^b	activity (scaled) ^c	$\text{N}\bullet$ formed (% initial $\text{Y}\bullet$) ^d	dCDP/ $\alpha 2$ ^e
$\text{Y}_{730}\text{NH}_2\text{Y}-\alpha 2^f$		156 ± 36	0.3–0.6	4–8		16	0.70
(His) ₆ - $\text{Y}_{730}\text{NH}_2\text{Y}-\alpha 2$		78 ± 12	0.2–0.3	3–4		14	0.70
$\text{Y}_{731}\text{NH}_2\text{Y}-\alpha 2^f$		175 ± 50	0.4–0.7	5–9		15	0.65
$\text{Y}_{356}\text{NH}_2\text{Y}-\beta 2$	0.5	305 ± 38	0.4–0.5	4–5	10–12	15	ND ^g

^a Average and standard deviation of 3–5 assays conducted on 2 or more independent enzyme isolations. ^b 2500 nmol/min/mg for wt- $\alpha 2$, 2200 nmol/min/mg for (His)₆- $\alpha 2$, 7000 nmol/min/mg for wt- $\beta 2$. ^c Scaled for radical content (0.5 $\text{Y}\bullet/\beta 2$ in mutant vs 1.2 $\text{Y}\bullet/\beta 2$ in wt). ^d N_3ADP was the substrate for $\text{Y}_{730}\text{NH}_2\text{Y}-\alpha 2$ and $\text{Y}_{731}\text{NH}_2\text{Y}-\alpha 2$, while N_3CDP was the substrate for (His)₆- $\text{Y}_{730}\text{NH}_2\text{Y}-\alpha 2$ and $\text{Y}_{356}\text{NH}_2\text{Y}-\beta 2$. Error in EPR spin quantitation is ~3% of the initial $\text{Y}_{122}\bullet$. ^e Determined by a hand-quench single turnover assay, as described in the text. ^f First described in ref 17. ^g Not determined.

of $\text{NH}_2\text{Y}\bullet$ formation in the three NH_2Y -RNRs with all S/E pairs is described below.

Catalytic Activity of $\text{Y}_{356}\text{NH}_2\text{Y}-\beta 2$. Initial experiments indicated that $\text{Y}_{730}\text{NH}_2\text{Y}-\alpha 2$ and $\text{Y}_{731}\text{NH}_2\text{Y}-\alpha 2$ catalyze dNDP production, despite the introduction of a ~190 mV thermodynamic hole in the PCET pathway.¹⁷ Activity assays revealed that $\text{Y}_{356}\text{NH}_2\text{Y}-\beta 2$ also catalyzes dCDP formation with 4–5% the activity of wt- $\beta 2$ (Table 1). When scaled for radical content ($\text{Y}_{356}\text{NH}_2\text{Y}-\beta 2$ contains 0.5 $\text{Y}\bullet/\beta 2$ vs 1.2 $\text{Y}\bullet/\beta 2$ in wt), the activity is 10–12% that of wt.

Since RNR is essential for *E. coli* viability, expression of NH_2Y -RNRs is always accompanied by endogenous levels of wt- $\alpha 2$ or $\beta 2$.³⁴ Additional contamination by wt RNR can arise from the misincorporation of Y in response to the nonsense codon due to imperfect substrate specificity by the NH_2Y -RS. Thus, three types of experiments were carried out to ensure that the reductase activity measured is associated with NH_2Y -RNRs.

A. N_3CDP Inactivation of NH_2Y -RNRs. Studies with wt RNRs have shown that N_3CDP is a stoichiometric inhibitor that requires $\text{C}_{439}\bullet$ -mediated 3'-hydrogen atom abstraction from the nucleotide prior to RNR inactivation. A nitrogen-centered nucleotide radical ($\text{N}\bullet$) is formed and covalently bound to the active site.^{23,26} Complete enzyme inactivation results after a 50% conversion of $\text{Y}_{122}\bullet$ to $\text{N}\bullet$, in agreement with the proposed half-site reactivity of RNR.^{7,8} Thus, if the 4–5% activity measured with $\text{Y}_{356}\text{NH}_2\text{Y}-\beta 2$ is associated with contaminating wt- $\beta 2$, 2–2.5% of the $\text{Y}\bullet$ would be converted to $\text{N}\bullet$. Observation of a larger percentage of $\text{N}\bullet$ would be indicative of activity inherent to $\text{Y}_{356}\text{NH}_2\text{Y}-\beta 2$. Thus, $\text{Y}_{356}\text{NH}_2\text{Y}-\beta 2$ was reacted with wt- $\alpha 2$, N_3CDP , and ATP, quenched at 1 min, and analyzed by EPR

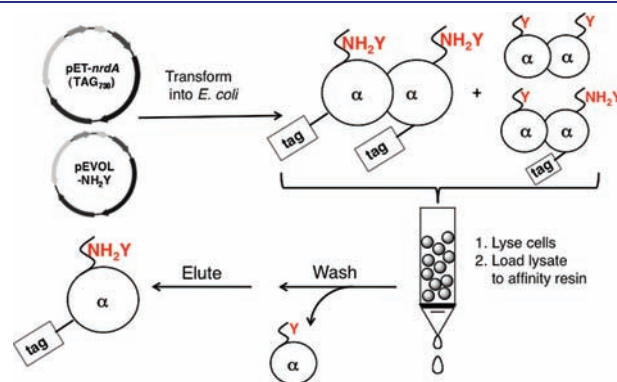


Figure 3. Strategy employed for removal of endogenous levels of wt- $\alpha 2$ and heterodimers of α and mutant α from $\text{NH}_2\text{Y}-\alpha 2$ samples. An N-terminal affinity tag on the mutant protein allows separation of the recombinant α from endogenous α via affinity chromatography under conditions in which the protein exists in an equilibrium between monomer (α) and dimer ($\alpha 2$).

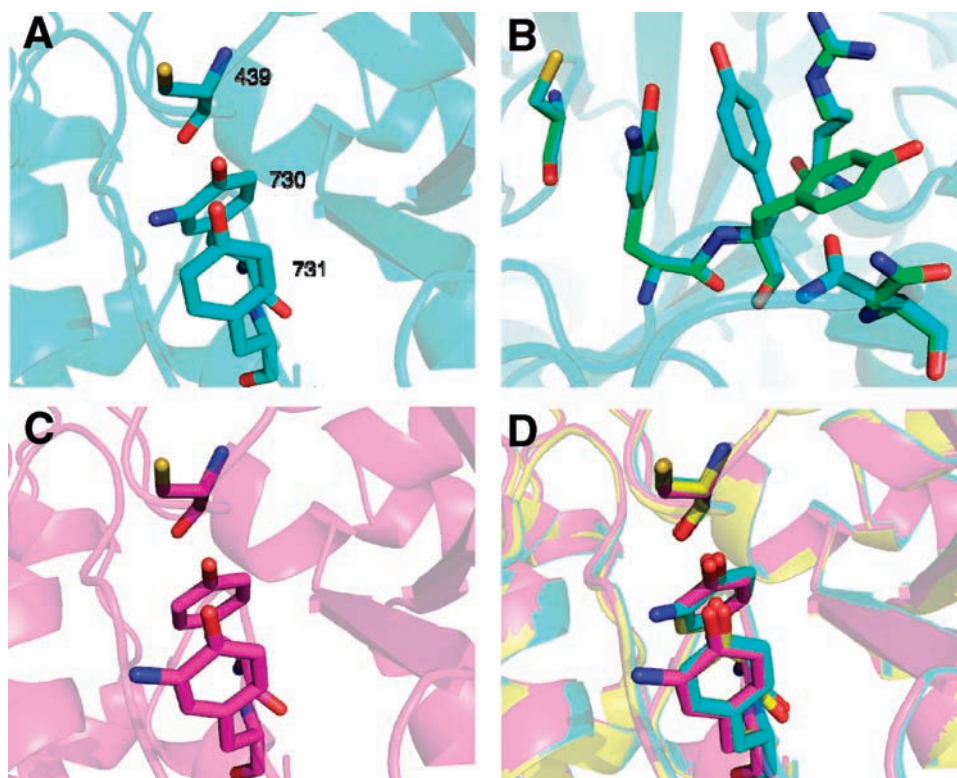


Figure 4. Crystal structures of $\text{NH}_2\text{Y-}\alpha_2\text{s}$. Oxygens are colored red, nitrogens, blue, and sulfurs, yellow. (A) Primary conformation assumed by residues of the PCET pathway in $\text{Y}_{730}\text{NH}_2\text{Y-}\alpha_2$ (2.5 Å resolution). (B) Electron density suggests a secondary conformation (green) present in the $\text{Y}_{730}\text{NH}_2\text{Y-}\alpha_2$ crystal in which the phenol of Y_{731} is oriented away from $\text{NH}_2\text{Y}_{730}$ and toward the protein surface, placing a distance of 9.5 Å between the phenolic oxygens. This movement is accompanied by changes at R_{411} and N_{733} (shown in sticks), and highlights the dynamic motion possible at the surface believed to participate in α_2/β_2 subunit interactions. (C) Primary conformation assumed by residues of the PCET pathway in $\text{Y}_{731}\text{NH}_2\text{Y-}\alpha_2$ (2.7 Å resolution). A second conformation, in which the NH_2 group is oriented on the right side of the phenol, is observed in one of the three molecules in the asymmetric unit. (D) Overlay of the structures of $\text{Y}_{730}\text{NH}_2\text{Y-}\alpha_2$ (cyan) and $\text{Y}_{731}\text{NH}_2\text{Y-}\alpha_2$ (magenta) with wt- α_2 (yellow, 2.3 Å resolution) solved under the same conditions demonstrates minimal perturbation of the PCET pathway in the predominant conformations assumed by the two mutants. Distances of 3.2–3.4 Å separate the phenolic oxygens of residues 730 and 731, and distances of 3.5–3.7 Å separate the sulfhydryl of 439 and the phenol of 730. Figure generated in PyMol from PDB-IDs 2x0x, 2x04, and 2x05.

spectroscopy (Figure S3 of SI). No spin was lost during the reaction, with 56% of the spin associated with $\text{Y}\bullet$, 28% with $\text{NH}_2\text{Y}\bullet$, and 16% with $\text{N}\bullet$ (Table 1). The amount of $\text{N}\bullet$ is six times higher than predicted on the basis of wt contamination, providing support for $\text{Y}_{356}\text{NH}_2\text{Y-}\beta_2\text{'s}$ activity. This result is consistent with previous inactivation assays of $\text{Y}_{730}\text{NH}_2\text{Y-}\alpha_2$ and $\text{Y}_{731}\text{NH}_2\text{Y-}\alpha_2$ (Table 1).¹⁷

B. Affinity Purification and Catalytic Activity of N-Terminally Tagged $\text{NH}_2\text{Y-RNRs}$. In an attempt to remove endogenous levels of wt subunit contamination, N-terminally affinity-tagged $\text{NH}_2\text{Y-RNRs}$ were constructed. Since α is an equilibrium mixture of monomer and dimer in the absence of nucleotides, recombinant, tagged $\text{NH}_2\text{Y-}\alpha_2$ should be separable from wt- α_2 via affinity chromatography (Figure 3). A number of StrepII- or $(\text{His})_6$ -tagged *nrdA* expression constructs with variable linker regions (0–10 amino acids) were constructed and the encoded proteins expressed and purified (Table S1 of SI). An N-terminal $(\text{His})_6$ tag and 10 amino acid linker gave the maximum yield, purity, and activity of all the tagged wt- $\alpha_2\text{s}$ investigated. This construct and the improved pEVOL³⁵ vector encoding the tRNA/ $\text{NH}_2\text{Y-RS}$ were used to express $(\text{His})_6\text{-Y}_{730}\text{NH}_2\text{Y-}\alpha_2$, and the resulting protein was purified to homogeneity (Figure S4 of SI). MALDI-TOF MS of the purified protein gave a major peak corresponding to the full-length protein with a single NH_2Y incorporated

(observed, 87 975 Da, predicted + Na^+ , 87 976 Da). The only other observable peak corresponded to 729-truncated protein. Further characterization of $(\text{His})_6\text{-Y}_{730}\text{NH}_2\text{Y-}\alpha_2$ by EPR (Figure S5 of SI) and SF UV-vis experiments monitoring $\text{NH}_2\text{Y}\bullet$ formation gave results almost identical to those with the untagged mutant.¹⁷ Thus, this construct was adopted for all future experiments. The affinity tagging strategy was extended to the β_2 subunit (Table S2 of SI), but the yield and/or radical content of the N-terminally StrepII- and $(\text{His})_6$ -tagged $\text{Y}_{356}\text{NH}_2\text{Y-}\beta_2$ mutants was low relative to that of untagged $\text{Y}_{356}\text{NH}_2\text{Y-}\beta_2$ and thus study of tagged $\text{NH}_2\text{Y-}\beta_2\text{s}$ was not pursued further.

Tagged $\text{NH}_2\text{Y-RNRs}$ were assayed for nucleotide reductase activity and were found to be catalytically active, with the results summarized in Table 1 and Tables S1 and S2 of the SI. $(\text{His})_6\text{-Y}_{730}\text{NH}_2\text{Y-}\alpha_2$ has $\sim 50\%$ the activity of the untagged mutant and demonstrates a narrower range of activities. Thus, the tagging procedure appears to have been successful in removing varying levels of contaminating wt. Additionally, $(\text{His})_6\text{-Y}_{730}\text{NH}_2\text{Y-}\alpha_2$ generates seven times more $\text{N}\bullet$ in the N_3CDP assay than can be rationalized on the basis of wt contamination (Table 1 and Figure S6 of the SI).

C. Single Turnover Assays for dCDP Formation. As a final test of catalysis, a hand-quenched single-turnover experiment was

conducted using $Y_{730}NH_2Y-\alpha 2$ (or $(His)_6-Y_{730}NH_2Y-\alpha 2$), wt- $\beta 2$, $[S-^3H]CDP$, and ATP. Under the reaction conditions employed, wt- $\alpha 2$ generates ~ 3 dCDP/ $\alpha 2$.⁷ Thus, a sample of $Y_{730}NH_2Y-\alpha 2$ with 4% wt activity, in which all of the activity is associated with contaminating wt RNR, should generate 0.12 dCDP/ $\alpha 2$. Both $Y_{730}NH_2Y-\alpha 2$ and $(His)_6-Y_{730}NH_2Y-\alpha 2$ generated 0.7 dCDP/ $\alpha 2$, or 6-fold more product than would be predicted for activity originating solely from contaminating wt (Table 1). A similar experiment with $Y_{731}NH_2Y-\alpha 2$ yielded 0.65 dCDP/ $\alpha 2$, whereas a control experiment using a redox-inactive $Y_{731}F$ mutant generated 0.09 dCDP/ $\alpha 2$, consistent with 3% contaminating wt in the latter sample. At present, the basis for substoichiometric formation of dCDP by NH_2Y -RNRs under single-turnover conditions is not understood. However, this observation is consistent with the results of single-turnover N_3CDP assays, in which only $\sim 1/3$ of the $NH_2Y\bullet$ formed is converted to $N\bullet$ during a one minute reaction, as described above. Collectively, the steady-state and single-turnover activity assays of both untagged and tagged NH_2Y -RNRs (Table 1 and Tables S1 and S2 of the SI) and the high accumulation of $N\bullet$ in all mutants (Table 1) provide convincing evidence that NH_2Y -RNRs catalyze dNDP formation.

Structural Characterization of $Y_{730}NH_2Y-\alpha 2$ and $Y_{731}NH_2Y-\alpha 2$. To determine whether incorporation of NH_2Y structurally perturbs the PCET pathway, $Y_{730}NH_2Y-\alpha 2$ and $Y_{731}NH_2Y-\alpha 2$ were crystallized, their structures determined by molecular replacement, and refined to 2.5 and 2.7 Å resolution, respectively (Table S3 of SI). As the starting model, a 2.3 Å structure of wt- $\alpha 2$ crystallized under similar conditions was used.¹¹ In all cases, the asymmetric unit contains $\alpha 2$ (molecules A and B), to which is appended a third α (molecule C). This third α also forms a true dimer in the crystal lattice. The major conformation assumed by $Y_{730}NH_2Y-\alpha 2$ (Figure 4A) is one in which the NH_2 substitution is oriented to the left when looking toward C_{439} from Y_{731} and the protein surface. Thus, the NH_2 group is situated toward the sterically less-dense side, and its opportunities for intermolecular hydrogen bonding to other residues are minimized. A similar conformation has been reported for the NO_2 group in the crystal structure of $Y_{730}NO_2Y-\alpha 2$.¹¹ Interestingly, additional electron density in the structure of $Y_{730}NH_2Y-\alpha 2$ suggests that Y_{731} can undergo a flipping motion away from $Y_{730}NH_2Y$ toward the protein surface, placing a distance of 9.5 Å between the phenolic oxygens of NH_2Y_{730} and Y_{731} (Figure 4B, green). Concomitant with this flipping are reorientations of N_{733} and R_{411} . This reorientation is provocative in that it highlights the dynamic flexibility of residues at the proposed $\alpha 2/\beta 2$ interface and suggests motions that may be possible upon subunit interactions. In the deposited structure, one molecule (C) in the asymmetric unit is built in the flipped conformation. A water molecule, present in the wt structure and hydrogen bonded to NH_2Y_{730} , Y_{413} and D_{334} , is also present in this structure, as well as an additional water hydrogen-bonded to Y_{731} .

The major conformation of the residues in the PCET pathway observed in the $Y_{731}NH_2Y-\alpha 2$ crystal is shown in Figure 4C. Similar to the 730 mutant, the NH_2 group is oriented to the left and does not interact with any surrounding residues. An analogous conformation has been reported for the NO_2 group of $Y_{731}NO_2Y-\alpha 2$.¹¹ However, in one of the three α monomers (B), the NH_2 substituent is oriented to the right, within hydrogen-bonding distance (2.5 Å) of the adjacent Y_{413} . In molecule C, a water with high occupancy is hydrogen-bonded to the OH groups of residues 730 and 731 as well as to the NH_2 group of

NH_2Y_{731} . Higher resolution structures are necessary to determine the role(s) for ordered waters in the PCET pathway.

An overlay of the wt structure with the most common conformations of the $Y_{730}NH_2Y-\alpha 2$ and $Y_{731}NH_2Y-\alpha 2$ structures is shown in Figure 4D and reveals no significant perturbations among the three structures in the distance between the phenolic oxygens of the residues at 730 and 731 (3.2–3.4 Å) and the distance between the phenolic oxygen of residue 730 and the sulfur of C_{439} (3.5–3.7 Å). In general, the structures reveal no major surprises and suggest that the redox pathway remains intact upon NH_2Y substitution. However, catalysis involving PCET is dependent on 0.1 Å changes and thus functionally informative structures require the presence of β , S and E, all of which are absent from the structures reported herein.

$NH_2Y\bullet$ Formation with S/E Pairs Monitored by EPR Spectroscopy. We have previously reported $NH_2Y\bullet$ formation and its detection by EPR methods in the reaction of $Y_{730}NH_2Y-\alpha 2$ or $Y_{731}NH_2Y-\alpha 2$ with wt- $\beta 2$, CDP and ATP quenched at 10–20 s.^{17,33} We now report similar studies on the reaction of $Y_{730}NH_2Y-\alpha 2$ and $Y_{731}NH_2Y-\alpha 2$ with wt- $\beta 2$ and the physiologically relevant S/E pairs (GDP/TTP, ADP/ATP/dGTP, UDP/ATP), with the samples hand-quenched at 20 s. The concentrations of S and E were chosen to saturate the nucleotide binding sites on $\alpha 2$. When examining ADP, both dGTP and ATP effectors were used,³⁶ as the presence of ATP makes the behavior of ADP/dGTP more closely mimic all other S/E pairs.

The spectra for the reactions with $Y_{730}NH_2Y-\alpha 2$ are shown in Figure S7a of the SI and are composites of $Y_{122}\bullet$ and $NH_2Y\bullet$. Subtraction of the $Y_{122}\bullet$ spectrum yields an $NH_2Y\bullet$ spectrum, with the latter species accounting for 47–53% of the total spin at 20 s. The $NH_2Y\bullet$ spectrum shows very little variation with different S/E pairs. The spectra for the reactions with $Y_{731}NH_2Y-\alpha 2$ are similar, with 27–45% of the spin at 20 s associated with $NH_2Y\bullet$ (Figure S7b of SI). In all cases, 20–30% of the total initial spin was lost in the first 20 s, suggesting that rapid freeze-quench (RFQ) techniques are preferable for future EPR analysis of these and similar reactions.

Kinetics of $NH_2Y\bullet$ Formation with S/E Pairs Monitored by SF UV–Vis Spectroscopy. SF UV–vis kinetic experiments monitoring $NH_2Y\bullet$ formation and $Y\bullet$ loss were carried out with all three NH_2Y -RNRs and all S/E pairs. In all cases, $NH_2Y\bullet$ formation was biphasic and occurred concomitantly with $Y_{122}\bullet$ loss (Table 2). The fast rate constant, k_{fast} , varied from 9–45 s⁻¹ and demonstrated a small dependence on position within the pathway with both k_{fast} and the conversion amplitude decreasing slightly with increasing distance between NH_2Y and $Y_{122}\bullet$. The average k_{fast} for all S/E pairs with NH_2Y at position 356, 731, and 730 is 38 s⁻¹ (22% conversion), 19 s⁻¹ (20%), and 14 s⁻¹ (15%), respectively. k_{fast} also demonstrates a small dependence on the S/E pair, with purines giving rise to faster rate constants than pyrimidines (GDP/TTP \approx ADP/dGTP/ATP > CDP/ATP > UDP/ATP). In contrast to the fast phase, the slow phase is nearly invariant with position and S/E pair, with an average k_{slow} of ~ 2.5 s⁻¹. We believe that both rate constants measure protein conformational changes rather than chemical events; our hypothesis is that k_{slow} reports on conformational changes preceding catalysis that are rate-determining in the wt enzyme,⁷ as described in the Discussion.

In the SF UV–vis experiments, 30–40% of $Y_{122}\bullet$ is converted to $NH_2Y\bullet$ over the two phases. This conversion is in good agreement with the conversion of total initial $Y_{122}\bullet$ to $NH_2Y\bullet$ (31–41%) in the hand-quench EPR experiments described

Table 2. Kinetics of NH₂Y• Formation in β2 and α2 at 25 °C with Different S/E Pairs Monitored by SF UV-Vis

substrate/effector	NH ₂ Y ₃₅₆ •		NH ₂ Y ₇₃₁ •		NH ₂ Y ₇₃₀ •	
	<i>k</i> (s ⁻¹) ^a	A (%)	<i>k</i> (s ⁻¹)	A (%)	<i>k</i> (s ⁻¹)	A (%)
CDP/ATP						
Fast phase	36 ± 4	25 ± 2	18 ± 2	22 ± 2	12 ± 1	20 ± 2
Slow phase	2.1 ± 0.6	5 ± 1	2.5 ± 0.3	10 ± 1	2.4 ± 0.2	19 ± 2
UDP/ATP						
Fast phase	30 ± 7	11 ± 1	9.3 ± 1.6	15 ± 2	9.3 ± 1.7	8 ± 1
Slow phase	1.5 ± 0.8	2 ± 1	2.0 ± 0.2	22 ± 1	1.7 ± 0.1	20 ± 2
GDP/TTP						
Fast phase	38 ± 6	25 ± 2	28 ± 3	22 ± 2	18 ± 2	15 ± 2
Slow phase	1.8 ± 0.3	7 ± 1	2.3 ± 0.3	9 ± 1	2.3 ± 0.2	16 ± 2
ADP/dGTP/ATP						
Fast phase	46 ± 9	25 ± 2	20 ± 6	19 ± 3	16 ± 2	17 ± 1
Slow phase	3.6 ± 2.0	5 ± 1	5.0 ± 1.8	9 ± 3	2.4 ± 0.2	14 ± 1

^a Errors reported as the standard deviation of >5 SF traces.

above, and in a single RFQ-EPR experiment with Y₇₃₁NH₂Y-α2, wt-β2, CDP, and ATP.¹⁸ In the case of previous studies with Y₃₅₆DOPA-β2, a 50% conversion of initial Y₁₂₂• to DOPA• was reported, which is the maximum conversion one would predict on the basis of the enzyme's proposed half-site reactivity.⁸ The difference in accumulation between DOPA• and NH₂Y•s is not understood, but may reflect the difference in reduction potentials between the two amino acids.

Similar SF kinetic experiments were carried out on NH₂Y-RNRs with S or E alone to gain insight about how nucleotide binding conformationally gates PCET. All three NH₂Y-RNRs (Table S4 of SI) form NH₂Y• with S alone, but both *k*_{fast} and *k*_{slow} are reduced relative to those with the corresponding S/E pair. In the absence of E, purine substrates experience an average reduction in rate constants that is 2-fold greater than that of pyrimidines. Total amplitudes of NH₂Y• formation are reduced only moderately, with an average of 22% conversion over two phases, compared to a 30% average in the presence of S/E. In presence of E alone (Table S4 of SI), rate constants and amplitudes of NH₂Y• formation are dramatically decreased, supporting a role for S as the key factor in triggering radical propagation. Recent studies from our laboratory have suggested that the role of E is to maximize the amount of active enzyme complex and enhance *k*_{cat} by lowering the *K*_d for subunit interactions in the presence of a properly matched S/E pair (Hassan, Yokoyama, and Stubbe, unpublished results). The nature of the conformational changes induced upon E binding are not known, but it is likely that the NH₂Y probe is sensitive to these changes, resulting in modest enhancements of *k*_{cat} and conversion amplitude for NH₂Y• formation in the presence of S/E relative to S alone.

Finally, a comparison of the biphasic kinetics of NH₂Y₃₅₆• formation to the predominantly triphasic kinetics previously reported for DOPA₃₅₆• formation (Table S5 of SI) supports our hypothesis that the additional mutations required for the ELP method have increased the kinetic complexity of the Y₃₅₆DOPA-β2 reaction. The striking similarities in the rate constants and amplitudes between the fast phase for NH₂Y• formation and fastest phase for DOPA• formation suggest that this phase reports on a purely conformational event, as an ET

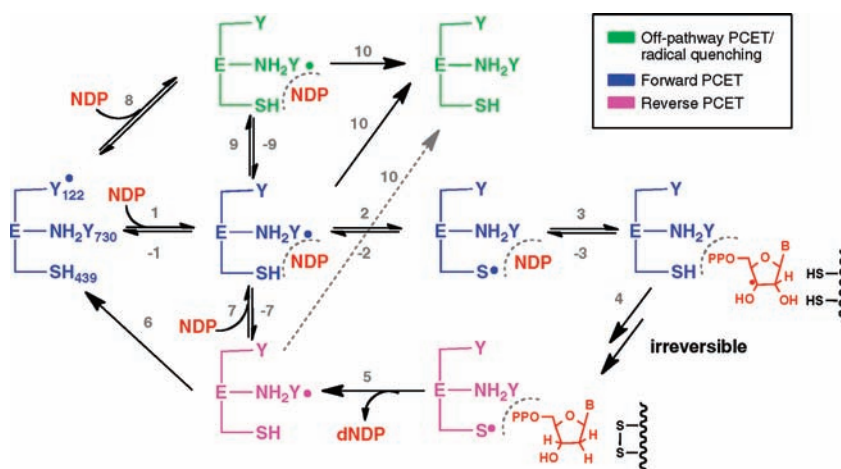
event would show correlation between the rate constant for radical formation and the redox potential of the unnatural amino acid at position 356.

Thus, NH₂Y fulfills two roles in studying PCET in *E. coli* RNR. First, its incorporation into three different positions on the pathway (Figure 1) has allowed for the kinetic characterization of intermediates formed during long-range radical propagation. Second, NH₂Y acts as a unique conformational probe, providing evidence for the role of S/E in conformational gating that is undetectable in the wt system.

DISCUSSION

NH₂Y-RNRs Are Catalytically Active. When studies on NH₂Y-RNRs were initiated, it was hypothesized that NH₂Y, ~190 mV easier to oxidize than Y at pH 7, would act as a thermodynamic sink, effectively trapping the radical during propagation and shutting down nucleotide reduction. This hypothesis was supported by previous studies on Y₃₅₆DOPA-β2, in which conversion of DOPA (~260 mV easier to oxidize than Y) to DOPA• rendered the enzyme completely inactive.⁸ It was further supported by experiments on Y₃₅₆F_nY-β2¹³ and NO₂Y-RNRs (Y₃₅₆NO₂Y-β2, Y₇₃₁NO₂Y-α2, and Y₇₃₀NO₂Y-α2),^{10,11} which indicated that a 200 mV increase in potential relative to Y prevents catalysis.

Thus, it was unexpected when all three NH₂Y-RNRs showed considerable catalytic activity (Table 1), as this implies that NH₂Y• is capable of the thermodynamically uphill oxidation of the next residue (Y or C) on the pathway (Figure 1). Given the important implications this observation has on the PCET mechanism, we made a considerable effort to establish that the observed activity is inherent to NH₂Y-RNRs and not associated with contaminating wt RNR. Since the genes coding for the subunits of RNR are essential in *E. coli*, the host organism for protein expression, endogenous levels of the wt subunits are always present at some level and thus can copurify with the recombinantly expressed protein. NH₂Y-RNR expression is sensitive to growth conditions and results in heterogeneity in the quality of NH₂Y-RNR isolated, as manifested by the large standard deviations in NH₂Y-RNR activities (Table 1). We

Scheme 1. Kinetic Model for $\text{NH}_2\text{Y}\cdot$ Formation and Nucleotide Reduction in $\text{NH}_2\text{Y-RNRs}^a$ 

^a The model for $\text{Y}_{730}\text{NH}_2\text{Y-}\alpha 2$ is shown, but similar models can be drawn for the 731 and 356 mutants by the addition of one or two Y oxidation steps within step 2 below. Enzyme species are colored according to three different pathways—forward PCET (blue), reverse PCET (magenta), and off-pathway PCET and/or radical quenching (green). The rate constants for individual steps, if available, are given in the text. Substrate (NDP) and product (dNDP) are shown in red. Effector is omitted from the scheme for clarity.

hypothesize that the activities at the higher end of these ranges (Table 1) are associated with protein isolated from growths with less successful expression, and contains a higher fraction of endogenous RNR. A similar argument has been made with $\text{NO}_2\text{Y-}\alpha 2\text{s}$.¹¹

An affinity purification protocol for an optimized tagged- $\alpha 2$, $\text{His}_6\text{-Y}_{730}\text{NH}_2\text{Y-}\alpha 2$, was developed (Figure 3) and the isolated protein assayed. This protein gave 50% lower activity and a narrower range of activities relative to untagged $\text{Y}_{730}\text{NH}_2\text{Y-}\alpha 2$ (Table 1). These results support our proposal that the endogenous wt- $\alpha 2$ that contaminates the latter sample has been largely removed from the former.

In application of the *in vivo* nonsense codon suppression method, the fidelity of the evolved tRNA/RS pair can introduce an additional mechanism by which wt RNR is produced. Both the K_m of the RS for the unnatural amino acid (UAA) and the relative abundance and availability of the UAA in the cell can influence the RS's selectivity for the UAA relative to Y. The fidelity of the tRNA/RS is also influenced by the expression system for the protein of interest, the position of UAA incorporation, and the growth medium. Since this source of contaminating wt protein is not removed by affinity purification, single-turnover experiments utilizing a native substrate (CDP) or a mechanism-based inhibitor (N_3CDP) were conducted on both the tagged and untagged $\text{NH}_2\text{Y-RNRs}$. In all cases, at least 4-fold more product (dCDP or $\text{N}\cdot$, respectively) was formed than can be rationalized on the basis of contaminating wt (Table 1, Figures S3 and S6). These single-turnover assays provide the strongest support for the high fidelity of the $\text{NH}_2\text{Y-RS/tRNA}$ pair and for the catalytic activity of $\text{NH}_2\text{Y-RNRs}$.

Kinetic Model for $\text{NH}_2\text{Y-RNRs}$. Our current model for catalysis by $\text{NH}_2\text{Y-RNRs}$ is shown in Scheme 1. While NH_2Y is drawn at position 730 of α , a similar mechanism incorporating an additional oxidation step(s) may be drawn if NH_2Y is located at position 731 of α or 356 of β . The model indicates that, in the presence of both $\alpha 2$ and $\beta 2$, the binding of S and E initiates radical propagation, as demonstrated by SF studies described above and previously.¹⁷ $\text{NH}_2\text{Y}\cdot$ formation occurs by two distinct pathways (steps 1 and 8) as revealed by its biphasic kinetics

(Figure 2). We assign the observed k_{fast} to step 8 (green pathway, Scheme 1) and propose that this rate constant reports on PCET between a pathway residue and $\text{Y}_{122}\cdot$, resulting in the formation of an $\text{NH}_2\text{Y}\cdot$ that is not in an appropriate conformation to oxidize C_{439} . It is likely that this electron excursion or “rattling” occurs in the wt RNR, but that the equilibrium lies strongly in favor of reoxidation of Y_{122} , the proposed thermodynamic minimum on the pathway. While this process is kinetically invisible in the wt enzyme, in the $\text{NH}_2\text{Y-RNRs}$, introduction of a new thermodynamic minimum on the pathway results in the rapid formation of a stable $\text{NH}_2\text{Y}\cdot$ with its rate constant for formation and accumulation dependent on position and S/E pair (Table 2). A similar event has been proposed to occur in the adenosylcobalamin-dependent class II RNR. Using a prochirally labeled 5'-deoxyadenosyl moiety of the cofactor, fast stereochemical scrambling of the label occurs, indicating rapid cleavage of the carbon–cobalt bond despite the inability to detect cob(II)alamin by rapid kinetic techniques.³⁷

$\text{NH}_2\text{Y}\cdot$ is also formed by step 1, with a k_{slow} of $\sim 2.5 \text{ s}^{-1}$ that we assign to the slow conformational gating step subsequent to S/E binding in which the protein assumes a conformation optimized for C_{439} oxidation. This assignment is supported by k_{slow} being independent of position and S/E pair (Table 2). This number falls within the lower range of values reported for the rate-determining conformational change in wt RNR ($2\text{--}10 \text{ s}^{-1}$),⁷ and may reflect changes induced by the NH_2Y substitution that could slow conformational priming, such as disruption of ordered water molecules or H-bonding networks. It is not yet known whether the two populations of $\text{NH}_2\text{Y}\cdot\text{s}$ formed in steps 1 and 8 interconvert (steps 9 and -9), but if they do, the interconversion must be slow ($< 2.5 \text{ s}^{-1}$) based on the observation of two distinct kinetic phases. It is possible that these states may interconvert on the time scale of steady-state turnover, and if so, both populations would be relevant to dCDP formation. RFQ methods in conjunction with EPR and ENDOR spectroscopies may be used to probe the existence, and possible interconversion, of the two $\text{NH}_2\text{Y}\cdot$ populations. The nature of the conformational changes associated with k_{slow} (1) and k_{fast} (8) are unknown, but they likely involve subtle reorientations to optimize radical

propagation. Temperature dependence and viscogen dependence studies may provide further evidence supporting the assignment of these rate constants to conformational changes.³⁸

We will argue subsequently that the next step, oxidation by $\text{NH}_2\text{Y}\bullet$ of the subsequent residue in the pathway (step 2), is the rate-limiting step in the steady state (0.2 to 0.7 s^{-1}). But first let us consider the remaining steps in Scheme 1. The chemistry of nucleotide reduction (steps 3 and 4) occurs rapidly (>100 to 300 s^{-1}) based on kinetic modeling of the wt system⁷ and recent experimental evidence using the mutant $\text{Y}_{122}\text{NO}_2\text{Y}\bullet\text{-}\beta 2$ as a radical initiator.³⁹ In this mutant, ET is decoupled from both PT and conformational gating, and dCDP is formed at $100\text{--}300\text{ s}^{-1}$. This rate constant is similar to the presteady-state rate constant for dCTP formation of 55 s^{-1} that has been measured in the *L. leichmannii* RNR.⁴⁰ Once dCDP is formed (step 4), reformation of the $\text{NH}_2\text{Y}\bullet$ by reverse PCET should be rapid ($\geq 100\text{ s}^{-1}$, magenta pathway, step 5). Evidence from single-turnover experiments using $\text{Y}_{122}\text{NO}_2\text{Y}\bullet\text{-}\beta 2$ also indicates that $\text{Y}_{356}\bullet$ is reformed with a rate constant of at least $100\text{--}300\text{ s}^{-1}$ following nucleotide reduction,³⁹ and kinetic simulations of the wt RNR mechanism require a comparably fast (if not faster) rate constant for reverse PCET.⁷

Our model provides two possible fates for the $\text{NH}_2\text{Y}\bullet$ generated upon reverse PCET (step 5). It can either reinitiate the nucleotide reduction process directly (step 7), or it can regenerate the $\text{Y}_{122}\bullet$ through step 6, or steps 7 and -1 . The latter two mechanisms would involve one or two transient $\text{Y}\bullet$ s and a $\text{W}\bullet$ as intermediates, depending on the position of NH_2Y on the pathway.^{5,6} While steps -1 and 6 are likely to be endergonic, we have previously demonstrated reverse PCET and slow reoxidation of Y_{122} by $\text{DOPA}_{356}\bullet$ and $\text{NH}_2\text{Y}_{356}\bullet$ only with the heterodimers $\text{Y}_{356}\text{DOPA-}\beta\beta'$ ³⁹ and $\text{Y}_{356}\text{NH}_2\text{Y-}\beta\beta'$ (Minnihan and Stubbe, unpublished results) with $\text{wt-}\alpha 2$, CDP, and ATP. Thus, steps -1 and/or 6 have thermodynamic precedent. However, reoxidation of $\text{Y}_{122}\bullet$ has never been observed in the relevant homodimers and thus a pathway in which $\text{NH}_2\text{Y}\bullet$ becomes the radical initiator for all subsequent turnovers (step 7 to step 2) must also be considered.

We now return to the slow steady-state rate constant for dNDP production by $\text{NH}_2\text{Y-RNRs}$ (0.2 to 0.7 s^{-1}) and consider two steps to which it may be assigned. It may be associated with reduction of the active-site disulfide (not shown in Scheme 1) formed concomitant with dCDP production (step 4), or with oxidation by $\text{NH}_2\text{Y}\bullet$ of the subsequent amino acid on the radical propagation pathway (step 2). Let us consider the first possibility. Under our assay conditions, wt RNR has a turnover number of $>2\text{ s}^{-1}$, more than four times faster than the steady-state rate constant of $\text{NH}_2\text{Y-RNRs}$. We think it is unlikely that substitution of NH_2Y for Y would alter the kinetics of disulfide reduction or conformational changes accompanying rereduction. Disulfide reduction has been proposed to be rate-limiting in *E. coli* wt RNR when assayed at high protein concentration ($k_{\text{cat}} = 1\text{ s}^{-1}$ at $[\alpha 2] > 1\text{ }\mu\text{M}$).⁷ Thus, steady-state assays were performed on $\text{Y}_{730}\text{NH}_2\text{Y-}\alpha 2$ over a 20-fold concentration range, encompassing the regimes in which disulfide reduction is and is not rate limiting for $\text{wt-}\alpha 2$. All concentrations yielded identical specific activity measurements for the mutant. Thus, the chemistry of disulfide reduction and the conformational reorganization necessary to prepare RNR for a second turnover seem unlikely to limit k_{cat} in $\text{NH}_2\text{Y-RNRs}$.

Thus, our favored candidate for the rate-determining step in the overall scheme is step 2, oxidation of subsequent residues in

the pathway by $\text{NH}_2\text{Y}\bullet$. One problem with this proposal arises from the three different locations of NH_2Y , and the resulting differences in the amino acid oxidized in step 2. As drawn in Scheme 1, $\text{NH}_2\text{Y}_{730}\bullet$ oxidizes C_{439} . However, $\text{NH}_2\text{Y}_{356}\bullet$ and $\text{NH}_2\text{Y}_{731}\bullet$ will oxidize Y_{731} and Y_{730} , respectively. We predicted that the oxidation of C_{439} by $\text{NH}_2\text{Y}_{730}\bullet$ would be the most endergonic of the three, and that this would be reflected in position-dependent differences in k_{cat} . This is not the case (Table 1), with the rate constants for $\text{Y}_{730}\text{NH}_2\text{Y-}\alpha 2$ and $\text{Y}_{731}\text{NH}_2\text{Y-}\alpha 2$ being identical within error. If step 2 is rate-determining, it is likely that the protein environment modulates the relative oxidation potentials of the pathway Ys and/or that the uphill oxidation of C_{439} is driven by coupling to rapid irreversible chemical step(s) during nucleotide reduction.

Finally, for the sake of completeness, Scheme 1 also includes the slow reduction of the $\text{NH}_2\text{Y}\bullet$ by a number of nonspecific pathways (step 10). This decay process (k_{red} of $0.004\text{--}0.007\text{ s}^{-1}$)⁴¹ is 100-fold slower than the steady-state turnover number and does not contribute to significant radical loss on the time scale of our experiments.

Our model (Scheme 1) makes testable predictions about radical formation and dNDP production in $\text{NH}_2\text{Y-RNRs}$. For instance, if step 2 is rate-limiting, a solvent kinetic isotope effect (KIE) should be apparent when any of the $\text{NH}_2\text{Y-RNRs}$ is assayed in D_2O . While interpretation of solvent isotope effects is always complicated, the ability to measure them at each step in the pathway will be mechanistically informative. Similarly, the rate constant for dCDP formation in the first turnover, determined by a rapid chemical-quench experiment, should be identical to that in the steady state. Alternatively, if dCDP is formed with a rate constant similar to $\text{NH}_2\text{Y}\bullet$ formation ($\sim 2.5\text{ s}^{-1}$), a step subsequent to dCDP formation (step 6 or 7, or disulfide reduction) must be rate-limiting. Finally, the ability to detect a catalytically active $\text{NH}_2\text{Y}\bullet$ at each position in the pathway is allowing high-field ENDOR spectroscopic experiments to be conducted to elucidate hydrogen-bonding networks relevant to coupling PT and ET events. These and other experiments are underway to challenge and refine the kinetic model for catalysis in $\text{NH}_2\text{Y-RNRs}$.

■ ASSOCIATED CONTENT

S Supporting Information. Generation of plasmids pTrc-*nrdB*, pTrc-*nrdB*(TAG₃₅₆), pEVOL-NH₂Y, pET-*nrdA*(wt) and pET-*nrdA*(TAG₇₃₀); expression and purification of N-Strep-Y₇₃₀NH₂Y- $\alpha 2$; expression and purification of N-Strep-Y₃₅₆NH₂Y- $\beta 2$ and (His)₆-Y₃₅₆NH₂Y- $\beta 2$; specific activities of tagged $\alpha 2$ s and Y₇₃₀NH₂Y- $\alpha 2$ s (Table S1); specific activities of tagged $\beta 2$ s and Y₃₅₆NH₂Y- $\beta 2$ s (Table S2); crystallization conditions and refinement statistics for structures of $\text{NH}_2\text{Y-}\alpha 2$ s (Table S3); kinetics of $\text{NH}_2\text{Y}\bullet$ formation in $\beta 2$ and $\alpha 2$ by SF UV-vis with S or E alone (Table S4); a comparison of the kinetics of radical formation in Y₃₅₆NH₂Y- $\beta 2$ and Y₃₅₆DOPA- $\beta 2$ (Table S5); SDS-PAGE of the expression and purification of Y₃₅₆NH₂Y- $\beta 2$ (Figure S1); ESI-MS of Y₃₅₆NH₂Y- $\beta 2$ (Figure S2); reaction of Y₃₅₆NH₂Y- $\beta 2$ with $\text{wt-}\alpha 2$, N₃CDP, and ATP monitored by EPR (Figure S3); SDS-PAGE of the expression and purification of (His)₆-Y₇₃₀NH₂Y- $\alpha 2$ (Figure S4); reaction of (His)₆-Y₇₃₀NH₂Y- $\alpha 2$ with $\text{wt-}\beta 2$, CDP, and ATP monitored by EPR (Figure S5); reaction of (His)₆-Y₇₃₀NH₂Y- $\alpha 2$ with $\text{wt-}\beta 2$, N₃CDP, and ATP monitored by EPR (Figure S6); and EPR spectra of $\text{NH}_2\text{Y}\bullet$ s formed with various S/E pairs (Figure S7).

This material is available free of charge via the Internet at <http://pubs.acs.org>.

AUTHOR INFORMATION

Corresponding Author

stubbe@mit.edu

Present Addresses

[†]Department of Biological Chemistry and Molecular Pharmacology, Harvard Medical School, 240 Longwood Avenue, Boston, MA 02115

ACKNOWLEDGMENT

We thank Dr. Kenichi Yokoyama for cloning pEVOL-NH₂Y and for thoughtful discussions. This work was supported by the NIH grant GM29595 (to J.S.).

REFERENCES

- (1) Stubbe, J.; van der Donk, W. A. *Chem. Rev.* **1998**, *98*, 705–762.
- (2) Jordan, A.; Reichard, P. *Annu. Rev. Biochem.* **1998**, *67*, 71–98.
- (3) Nordlund, P.; Reichard, P. *Annu. Rev. Biochem.* **2006**, *75*, 681–706.
- (4) Thelander, L. *J. Biol. Chem.* **1973**, *248*, 4591–4601.
- (5) Uhlin, U.; Eklund, H. *Nature* **1994**, *370*, 533–539.
- (6) Stubbe, J.; Nocera, D. G.; Yee, C. S.; Chang, M. C. Y. *Chem. Rev.* **2003**, *103*, 2167–2201.
- (7) Ge, J.; Yu, G.; Ator, M. A.; Stubbe, J. *Biochemistry* **2003**, *42*, 10071–10083.
- (8) Seyedsayamdost, M. R.; Stubbe, J. *J. Am. Chem. Soc.* **2006**, *128*, 2522–2523.
- (9) Seyedsayamdost, M. R.; Stubbe, J. *J. Am. Chem. Soc.* **2007**, *129*, 2226–2227.
- (10) Yee, C. S.; Seyedsayamdost, M. R.; Chang, M. C. Y.; Nocera, D. G.; Stubbe, J. *Biochemistry* **2003**, *42*, 14541–14552.
- (11) Yokoyama, K.; Uhlin, U.; Stubbe, J. *J. Am. Chem. Soc.* **2010**, *132*, 8385–8397.
- (12) Yee, C. S.; Chang, M. C. Y.; Ge, J.; Nocera, D. G.; Stubbe, J. *J. Am. Chem. Soc.* **2003**, *125*, 10506–10507.
- (13) Seyedsayamdost, M. R.; Yee, C. S.; Reece, S. Y.; Nocera, D. G.; Stubbe, J. *J. Am. Chem. Soc.* **2006**, *128*, 1562–1568.
- (14) Nordlund, P.; Sjöberg, B. M.; Eklund, H. *Nature* **1990**, *345*, 593–598.
- (15) Xie, J.; Schultz, P. G. *Methods* **2005**, *36*, 227–238.
- (16) DeFelippis, M. R.; Murthy, C. P.; Broitman, F.; Weinraub, D.; Faraggi, M.; Klapper, M. H. *J. Phys. Chem.* **1991**, *95*, 3416–3419.
- (17) Seyedsayamdost, M. R.; Xie, J.; Chan, C. T.; Schultz, P. G.; Stubbe, J. *J. Am. Chem. Soc.* **2007**, *129*, 15060–15071.
- (18) Seyedsayamdost, M. R.; Stubbe, J. *Methods Enzymol.* **2009**, *462*, 45–76.
- (19) Minnihan, E. C.; Seyedsayamdost, M. R.; Stubbe, J. *Biochemistry* **2009**, *48*, 12125–12132.
- (20) (a) Tommos, C.; Skalicky, J. J.; Pilloud, D. L.; Wand, A. J.; Dutton, P. L. *Biochemistry* **1999**, *38*, 9495–9507. (b) Throughout this manuscript, we cite 0.83 V as the E_p of Y at pH 7, as measured in ref 20a, as this is the value that has been independently confirmed in our lab (ref 10). It may be compared to a value of 0.93 V, as reported in ref 16 and references therein.
- (21) Jovanovic, S. V.; Steenken, S.; Tosic, M.; Marjanovic, B.; Simic, M. G. *J. Am. Chem. Soc.* **1994**, *116*, 4846–4851.
- (22) Salowe, S. P.; Stubbe, J. *J. Bacteriol.* **1986**, *165*, 363–366.
- (23) Salowe, S. P.; Ator, M. A.; Stubbe, J. *Biochemistry* **1987**, *26*, 3408–3416.
- (24) Chivers, P. T.; Prehoda, K. E.; Volkman, B. F.; Kim, B. M.; Markley, J. L.; Raines, R. T. *Biochemistry* **1997**, *36*, 14985–14991.
- (25) Russel, M.; Model, P. *J. Bacteriol.* **1985**, *163*, 238–242.
- (26) Salowe, S.; Bollinger, J. M., Jr.; Ator, M.; Stubbe, J.; McCracken, J.; Peisach, J.; Samano, M. C.; Robins, M. J. *Biochemistry* **1993**, *32*, 12749–12760.
- (27) Artin, E.; Wang, J.; Lohman, G. J.; Yokoyama, K.; Yu, G.; Griffin, R. G.; Bar, G.; Stubbe, J. *Biochemistry* **2009**, *48*, 11622–11629.
- (28) Bollinger, J. M., Jr.; Tong, W. H.; Ravi, N.; Huynh, B. H.; Edmondson, D. E.; Stubbe, J. A. *Methods Enzymol.* **1995**, *258*, 278–303.
- (29) Leslie, A. G. W. *Joint CCP4 and ESF-EACBM Newsletter; Daresbury Laboratory: Warrington, UK, 1992; Volume 26.*
- (30) Collaborative Computational Project *Acta Crystallogr., D: Biol. Crystallogr.* **1994**, *50*, 760–763.
- (31) Jones, T. A.; Zou, J. Y.; Cowan, S. W.; Kjeldgaard, M. *Acta Crystallogr., A* **1991**, *47*, 110–119.
- (32) Seyedsayamdost, M. R. PhD Thesis; Massachusetts Institute of Technology, 2007.
- (33) Seyedsayamdost, M. R.; Argirevic, T.; Minnihan, E. C.; Stubbe, J.; Bennati, M. *J. Am. Chem. Soc.* **2009**, *131*, 15729–15738.
- (34) Aberg, A.; Hahne, S.; Karlsson, M.; Larsson, A.; Ormo, M.; Ahgren, A.; Sjöberg, B. M. *J. Biol. Chem.* **1989**, *264*, 12249–12252.
- (35) Young, T. S.; Ahmad, I.; Yin, J. A.; Schultz, P. G. *J. Mol. Biol.* **2010**, *395*, 361–374.
- (36) Larsson, A.; Reichard, P. *J. Biol. Chem.* **1966**, *241*, 2540–2549.
- (37) Licht, S. S.; Booker, S.; Stubbe, J. *Biochemistry* **1999**, *38*, 1221–1233.
- (38) Patel, A. D.; Nocek, J. M.; Hoffman, B. M. *J. Phys. Chem. B* **2008**, *112*, 11827–11837.
- (39) Yokoyama, K.; Uhlin, U.; Stubbe, J. *J. Am. Chem. Soc.* **2010**, *132*, 15368–15379.
- (40) Licht, S. S.; Lawrence, C. C.; Stubbe, J. *J. Am. Chem. Soc.* **1999**, *121*, 7463–7468.
- (41) Seyedsayamdost, M. R.; Yee, C. S.; Stubbe, J. *Biochemistry* **2011**, *50*, 1403–1411.